Journal of
Ceramic Science
and Technology

J. Ceram. Sci. Technol., **11** [2] 103-110 (2020)
DOI: 10.4416/JCST2020-00012
available online at: http://www.ceramic-science.com

The Synthesis of Multi-Layer Silver, Copper and Aluminum Thick Films on Alumina Substrates using a Screen-Printing Method

Jun Fang*[1, 2], Renli Fu[1], Xiguang Gu[1], Xinyao Zhang[1], Guojun Li[1]

[1]College of Materials Science and Technology, Nanjing University of Aeronautics and Astronautics, Nanjing 211106, China
[2]Nanjing Miko Electronic Technology Co., Ltd, Nanjing 211235, China

received April 27, 2020; received in revised form June 23, 2020; accepted June 24, 2020

Abstract

The thick-film surface metallization of alumina substrates was performed by means of a screen-printing method. The Ag-Ag, Ag-Cu and Ag-Al multi-layer circuits were constructed on the surface of alumina substrates, respectively. The microstructure and image diffusion of the interface have been determined with SEM and EDS. Our results suggest that Ag-Ag and Ag-Cu layers can form effective metallurgical bonding after sintering, whereas there is only a direct mechanical contact interface for the Ag-Al layer. The adhesion of the three interfaces is also different. The Ag-Ag layer exhibited the highest adhesion with more than 80 N, while the adhesion of Ag-Al layer was less than 30 N. Moreover, the resistance measurement results demonstrated that the three different multi-layers possess the same conduction ability (1.4 Ω), except Ag-Cu group slightly increased to 1.8 Ω owing to the oxidation of copper, and their conduction mechanisms have been clearly clarified. The multi-layers can provide a promising application in radio frequency (RF), microresistors, LED and other fields.

Keywords: Multi-layer, silver, copper, aluminum, screen printing

I. Introduction

With the requirements for multi-functionality, small size and light weight in electronic devices, the density and the number of electronic components on the packaged substrate are rapidly increasing. Hence, the interconnection between the electronic components is a more serious and difficult problem with regard to packaging in the small space available [1, 2]. In order to solve this problem, three-dimensional (3D) packaging technologies are used directly packaged with bare chips and can realize multi-layer stacking in the vertical direction [3]. In this way, the electronic devices become smaller, lighter and perform better [4]. With integration of 3D packaging technologies into the circuit design, material and cost savings can be realized.

There are many advantages of using ceramic circuit board for 3D structures, such as high dielectric strength and high thermal conductivity [5]. Traditional methods for constructing circuits on ceramic require processes such as lithography and etching. However, direct printing technology (such as inkjet, screen printing) can directly print the metal paste onto the ceramic surface to form the circuit pattern. The process is more efficient, reduces the design cycle to the final product, and is more environmentally friendly [6,7]. Because of these advantages, many researchers are trying to expand its application in various fields, such as radio frequency applications [6], microresistors [8], geothermal well applications [9], etc. In screen printing, one method of direct printing, a printable paste is printed onto the substrate with the help of a screen mask, and then sintered at a high temperature of 500 – 1000 °C, so as to form a graphic circuit on the ceramic surface. In addition to the metal powder components (powder particles size of 5 μm), the screen printing paste also includes organic solvents, glass phase and additives for application to the device and to form a mechanical connection between the substrate and the paste [10]. Some functional layers can also be applied to the ceramic substrate, such as copper, silver, aluminum and other metals at present [11 – 13]. Screen printing has been used to apply silver and its alloy as highly effective electrode materials in thick-film hybrid integrated circuit [14, 15]. However, silver is easily sulfurized. Wang *et al*. have fabricated a bilayer structure of Ag and Al by means of electron-beam evaporation, followed by annealing in an appropriate atmosphere to form a AlxOyNz layer on the Ag layers, which can reduce the rate of Ag sulfidation [16]. Meanwhile, the electrode consisting of two different metal layers (e.g. Al-Ag, Au-Ag, etc.) can improve the mechanical and electrical contact [17]. The combination of silver with copper, indium or other metals also limits the migration of silver to some extent [18, 19]. Therefore, multi-layer metal structures are necessary to obtain good performance.

To date, the multi-layer metal structure has usually been fabricated by methods such as sputtering or physical vapor deposition [20, 21]. However, there is no research on the thick-film method for the two different metals. In

* Corresponding author: fangjun_0328@163.com

this paper, Ag-Ag, Ag-Cu and Ag-Al multi-layer electrodes were fabricated on the surface of alumina ceramics by means of screen printing. The co-fired behavior and the interface composition of these multi-layer electrodes were determined by means of a scanning electronic microscope (SEM) and energy-dispersive spectroscopy (EDS). The bonding mechanism of the interface layer between the multi-layer films was then discussed.

II. Experimental

The samples with different thick films on 96 % alumina substrate (from Fujian Huaqing) were prepared and cut into 54 x 54 mm squares. Guangzhou 3Focus F14015 silver thick-film paste, Heraeus C7403 copper thick-film paste, Shanxi Hualong HL-800W aluminum thick-film paste were used for formation of test stacks. Models of the multi-layers for resistance measurement and adhesion measurement were designed in order to evaluate the properties of the multi-layer metals (Fig. 1).

The semi-automatic screen-printing machine High-Precision Printer PHP-1212B supplied by Shanghai Hoting Screen was used for screen printing. The prints were realized on alumina substrates with 0.3 mm thickness steel plate by means of laser cutting (to ensure printing thickness above 30 µm, measured with a digital altimeter from Seiko Measuring Instruments). Paste material, film size and thickness of the stack samples are shown in Table 1.

The specific construction process was divided into two steps. For Stack 1, the first step was printing and firing the first layer of silver onto the surface of the alumina substrate. The second step consisted of printing and firing the second layer of silver onto the first silver layer. Usually, between each printing step, the paste films were left to stand for 20 minutes at room temperature and subsequently dried at 180 °C for 15 minutes to remove any organic solvents. The sintering equipment used was a mesh belt furnace. The rate of temperature rise was 10 K/min, and the holding time was 15 minutes in the 850 °C zone. The same process was applied for Stack 2 and Stack 3 as for Stack 1, except that copper and aluminum paste were printed in the second step, respectively. The sintering atmosphere for the silver paste and aluminum paste was an air atmosphere (oxygen percentage was 21 %), and that for the copper paste was a high-purity nitrogen atmosphere. The specific conditions for conditions are shown in Table 2.

The surface of the stacks was observed with a LEICA camera and the results are shown in Fig. 2. The microstructures, cross-sections of the stacks and elemental distribution were obtained with a scanning electronic microscope (SEM, Zeiss, EVO018) and subsequent energy-dispersive spectroscopy (EDS, Oxford Instruments). The samples were cut with a CO_2 laser along the length of the metal layer perpendicular to the surface of the substrate. Cross-section samples were then polished using diamond films to 1 µm surface roughness before being etched with diluted 3 % HF + HCl solution. The pull test was used to measure the adhesion between the first and second layers.

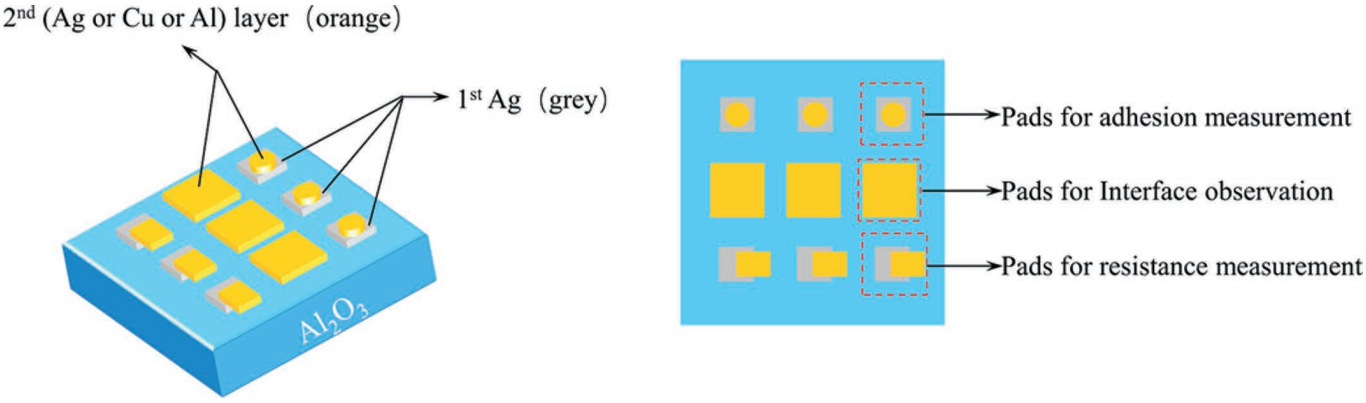

Fig. 1: Test pattern model of stacks.

Table 1: Details of the test stacks.

Sample	Layer	Paste	Thickness (µm)	Adhesion measurement	Resistance measurement
Stack 1	1st Ag	3Focus F14015	68	Square, 7x7 mm	Square, 7x7 mm
	2nd Ag	3Focus F14015	46	φ 5mm	5x7 mm
Stack 2	1st Ag	3Focus F14015	69	Square, 7x7 mm	Square, 7x7 mm
	2nd Cu	Heraeus C7403	42	φ 5mm	5x7 mm
Stack 3	1st Ag	3Focus F14015	65	Square, 7x7 mm	Square, 7x7 mm
	2nd Al	Hualong L800W	36	φ 5mm	5x7 mm

Table 2: The specific conditions for construction of the stacks.

Layer	Materials	Process	Stack 1	Stack 2	Stack 3
1st	Ag	Print + Dry	✓	✓	✓
		Firing (850 °C – 15 min)	✓	✓	✓
2nd	Ag	Print + Dry	✓		
		Firing (850 °C – 15 min)	✓		
	Cu	Print + Dry		✓	
		Firing (850 °C – 15 min) N_2 atmosphere		✓	
	Al	Print + Dry			✓
		Firing (550 °C – 10 min)			✓

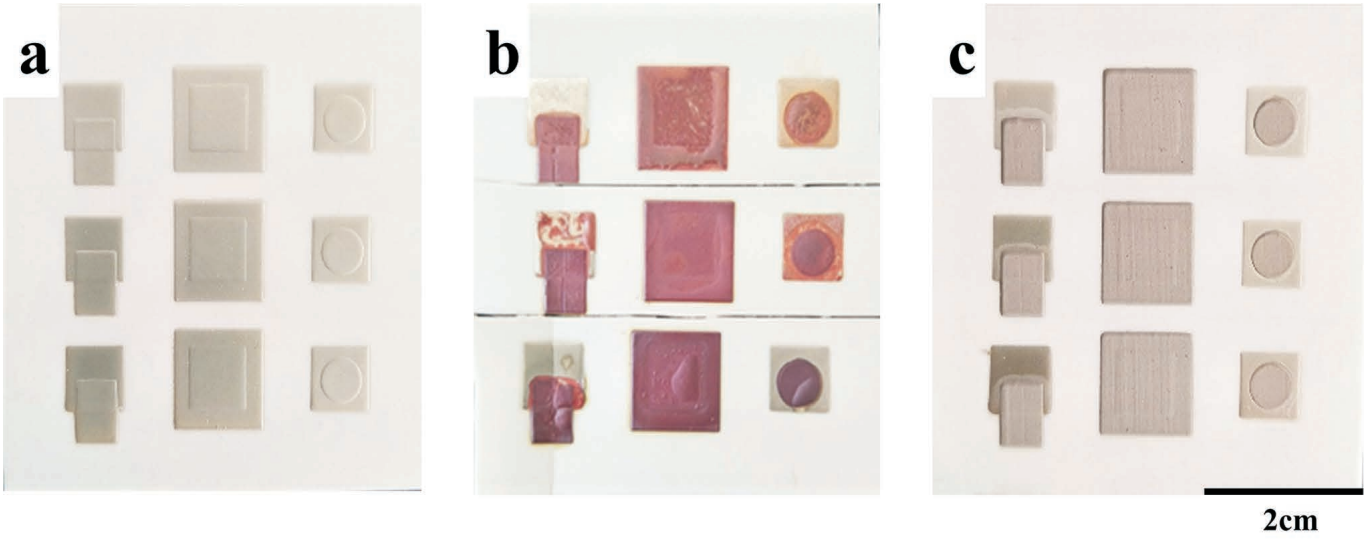

Fig. 2: Optical micrographs of test patterns for (a) Stack 1 (Ag-Ag), (b) Stack 2 (Ag-Cu) and (c) Stack 3 (Ag-Al).

The flat head screw and the second layer (circle in Fig. 1) to be tested were bonded together with resin, and then fixed on the test device. The testing device held the flat head screw, which was pulled out vertically to test the adhesion. The two probes of a multimeter were placed on two layers of metal in the test pattern to test the resistance. The results can describe the electrical connection between the multi-layer metals.

III. Results and Discussion

(1) The interface microstructure and cross-section of the multi-layer structure

The microstructures of the cross-section of stacks after sintering are shown in Fig. 3. After sintering, their interfaces are totally different. As shown in Fig. 3a, for Stack 1, SEM imaging showed mutual fusion between the first Ag layer and the second Ag layer, and the interface between the two Ag layers is not clearly distinguishable. This result demonstrated that they fuse well with each other. The multi-layer structure of Stack 2 (Fig. 3b) formed a single-layer structure and the interface layer disappeared. Ag and Cu melt together to form a remarkable bright and dark field region, and copper is surrounded by the silver. However, for Stack 3 (Fig. 3c), SEM imaging showed a distinct multi-layer structure composed of Ag layer and Al layer, similar to that before sintering, indicating that no obvious diffusion had occurred between the Ag layer and the Al layer.

(2) Interface reaction between different metal layers of the multi-layer structure

The microstructure of the cross-section of Stack 1 can be clearly seen from the partial area enlargement map (Fig. 4 a1). The first layer and the second layer of Ag have been fused and sintered together, but the interface region structure is looser than the sintered dense structure of the Ag layer owing to the granular materials and pores at the interface. The elemental distribution of Ag and Si in the cross-section after sintering is shown in the Fig. 4 b1. Both Ag and Si originate from silver paste, where the former is from the conductor and the latter is from the glass phase. It can be seen that the Ag from the Ag paste still forms a dense silver layer, while the glass phase originally belonging to the second Ag layer is scattered in the loose interface layer region, which can be

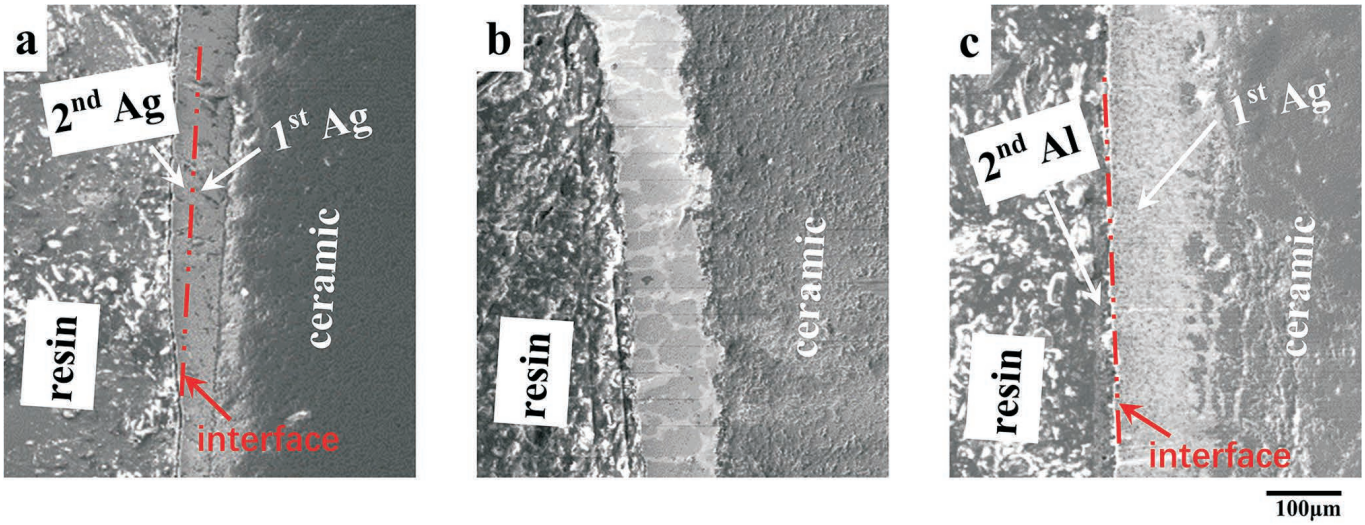

Fig. 3: SEM micrographs of cross-sections for (a) Stack 1 (Ag-Ag), (b) Stack 2 (Ag-Cu), and (c) Stack 3 (Ag-Al). The interface between different layers is highlighted with a red dash dot line.

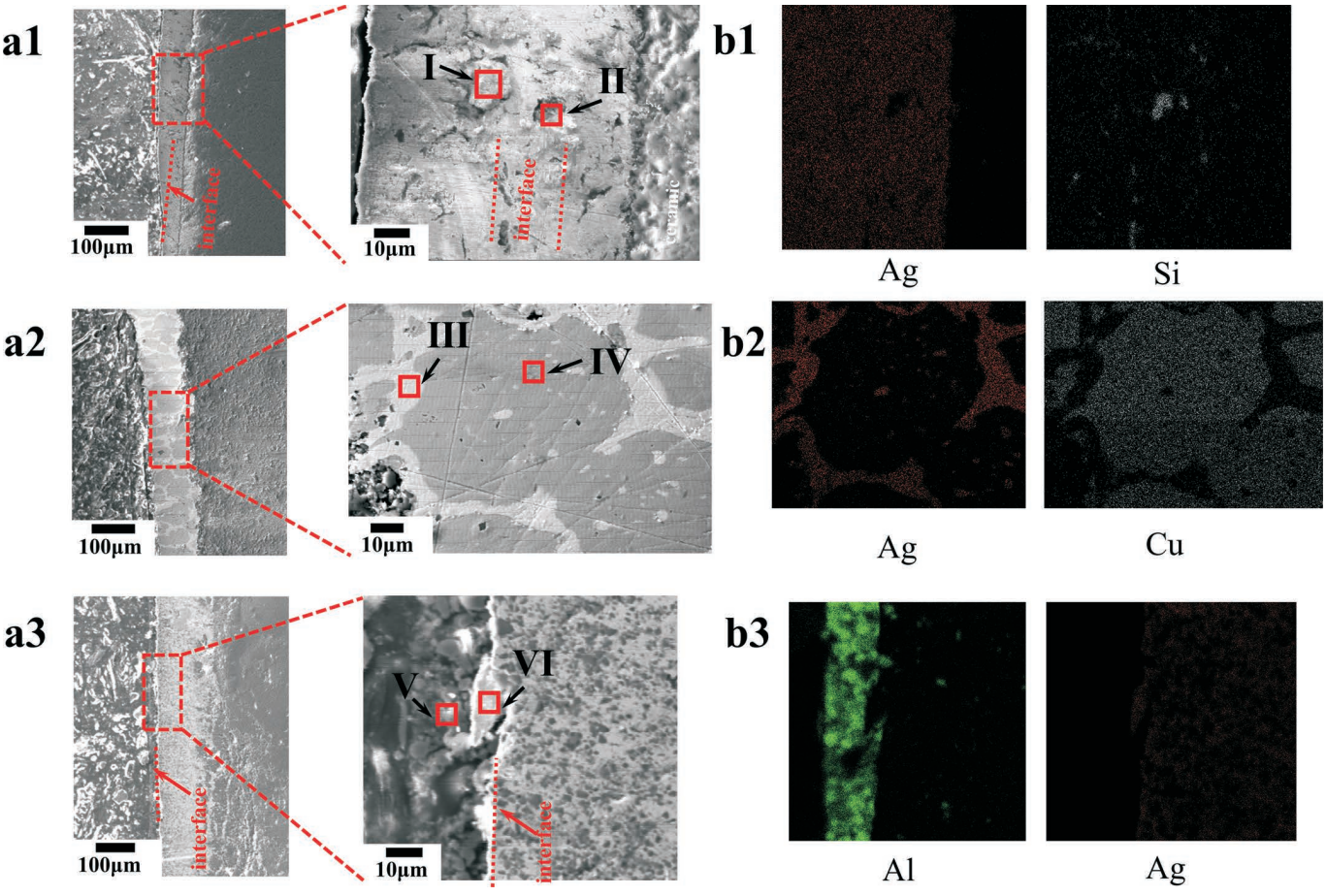

Fig. 4: Higher magnification SEM micrographs of a cross-section of (a1) Stack 1 (Ag-Ag), (a2) Stack 2 (Ag-Cu), (a3) Stack 3 (Ag-Al). The interface between the two layers is highlighted with red dashed lines. Elemental mapping by EDS of the same area revealed the distribution of Ag and Si, Ag and Cu, Ag and Al in the construction of the multi-layers (b1, b2 and b3).

proved by the distribution of the Si element in the cross-section. Fig. 5a shows the energy-dispersive spectrometer analysis of particles and voids marked as I and II (Fig. 4 a1) at the transition layer near the interface. The results show that the Ag layers belonging to the two Ag pastes can eventually form a dense silver layer and remains to be distributed at the interface in granular form. Meanwhile, the glass phase in the printed second Ag paste also fuses with that of the first Ag slurry. Ultimately, the two layers of silver paste can form a mutual amalgamation rather than the separation structure with the upper layer of silver and the bottom layer of glass phase in conventional sintering.

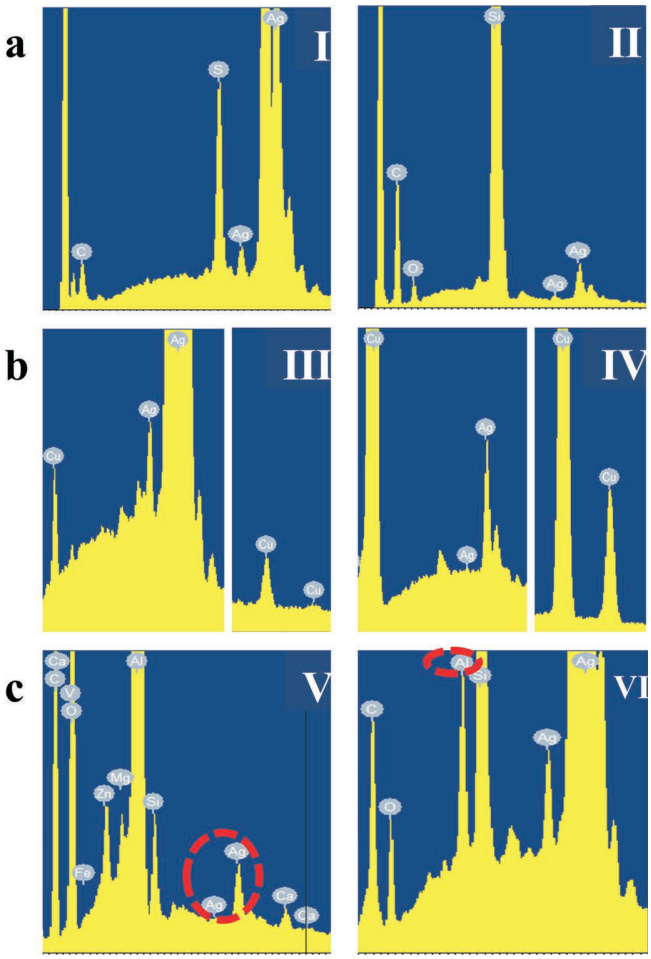

Fig. 5: The EDS elemental composition for (a) I and II in Fig. 4 a1, (b) III and IV in Fig. 4 a2, (c) V and VI in Fig. 4 a3.

The cross-section structure of Stack 2 is quite different from that of Stack 1, as shown in Fig. 4 a2. The first Ag layer and the second Cu layer have reacted completely with each other, and there is no multi-layer structure. Furthermore, the distribution of Ag and Cu elements in the cross-section shows that Cu is distributed in blocks while Ag is around them, as shown in the bright and dark regions. In Fig. 5b, the EDS of III and VI marked at Fig. 4 a2 shows that both bright and dark fields contain Cu and Ag, indicating they are Cu-Ag alloys. Therein the former is mainly composed of Ag and the latter mainly contains Cu, which is similar to the element mapping result in Fig. 4 b2. According to the Cu-Ag binary diagram, eutectic reaction between Cu and Ag occurs at 779 °C. Even though the Cu paste contains glass phase, the glass softens and flows during the heating process, and the eutectic reaction occurs when the Cu powder contacts with Ag at 779 °C. The glass phase fuses with the glass of the first layer of Ag in the bottom layer and is distributed at the interface between the metal layer and the ceramic, because no apparent glass phase is found in the metal layer or elsewhere.

As shown in Fig. 4 a3, unlike the former two stacks, Stack 3 exhibits a distinct multi-layer structure of Al and Ag layers with clear interfaces. It can be seen from the element mapping of Ag and Al (Fig. 4 b3) that the distribution of Al and Ag basically maintains the regional distribution after sintering, and there is almost no diffusion layer between them. Compared to the Ag layer, the Al layer is not continuous and dense, forming different sizes of metal particles. The EDS of a region marked in Fig. 5c shows that Mg, Si, Zn and many other elements are contained in the metal layer, most of them having originated from the glass phase in the Al paste. It shows that Al is distributed in the glass phase through the relative melting contact of oxide film after low-temperature (550 °C) sintering of the Al paste. In addition, Ag and Al are found in regions V and VI, indicating that there has still been slight diffusion between them, but not as obvious as with Ag and Cu. This diffusion may facilitate electrical conduction between the two layers, but it is not sufficient to form an effective reaction combination.

(3) Adhesive strength and resistance between the two layers of the multi-layer structure

The bonding strength between the different metal and Ag layers is shown in Fig. 6. Each system was constructed and measured six times to maintain stability. The bonding strength of the Ag-Ag and Ag-Al layers is stable. The former is higher, reaching more than 80 N, whereas the latter is relatively low, ranging from 20 to 25 N. However, the bonding strength of Cu-Ag layers shows some instability, some stacks falling off directly from the surface of ceramics. Some reaction in Stack 2 had formed defects such as bubbles, dissolution and copper oxidation, which would affect the adhesion of Ag-Cu (Fig. 3b).

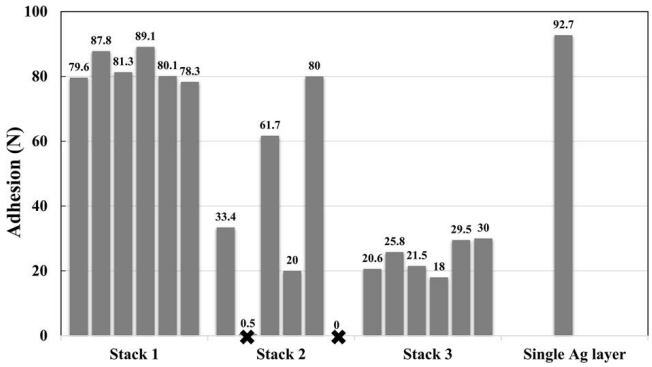

Fig. 6: The bonding strength between different metals with silver layers.

The two Ag layers fused with each other and had little influence on each other. The bonding strength of the two layers is slightly lower than that of the single Ag layer at 92 N owing to some fine holes between the two Ag layers. There is a direct contact interface with a little elemental diffusion and physical mechanical occlusion between the Ag layer and the Al layer. Therefore, it is not sufficiently dense to maintain a high enough bonding strength. Instead, eutectic reaction occurs sufficiently, and hence the test results reflect the bonding strength of the Ag-Cu alloy with alumina ceramics. Although the thermal expansion coefficients of Cu and Ag are not very different, after the alloy has been formed, the whole metal layer becomes thicker, the bubbles are formed along Stack 2, and the thermal expansion coefficients of the sintered glass phase are poorly matched, resulting in the instability of bonding strength owing to the different degrees of reaction.

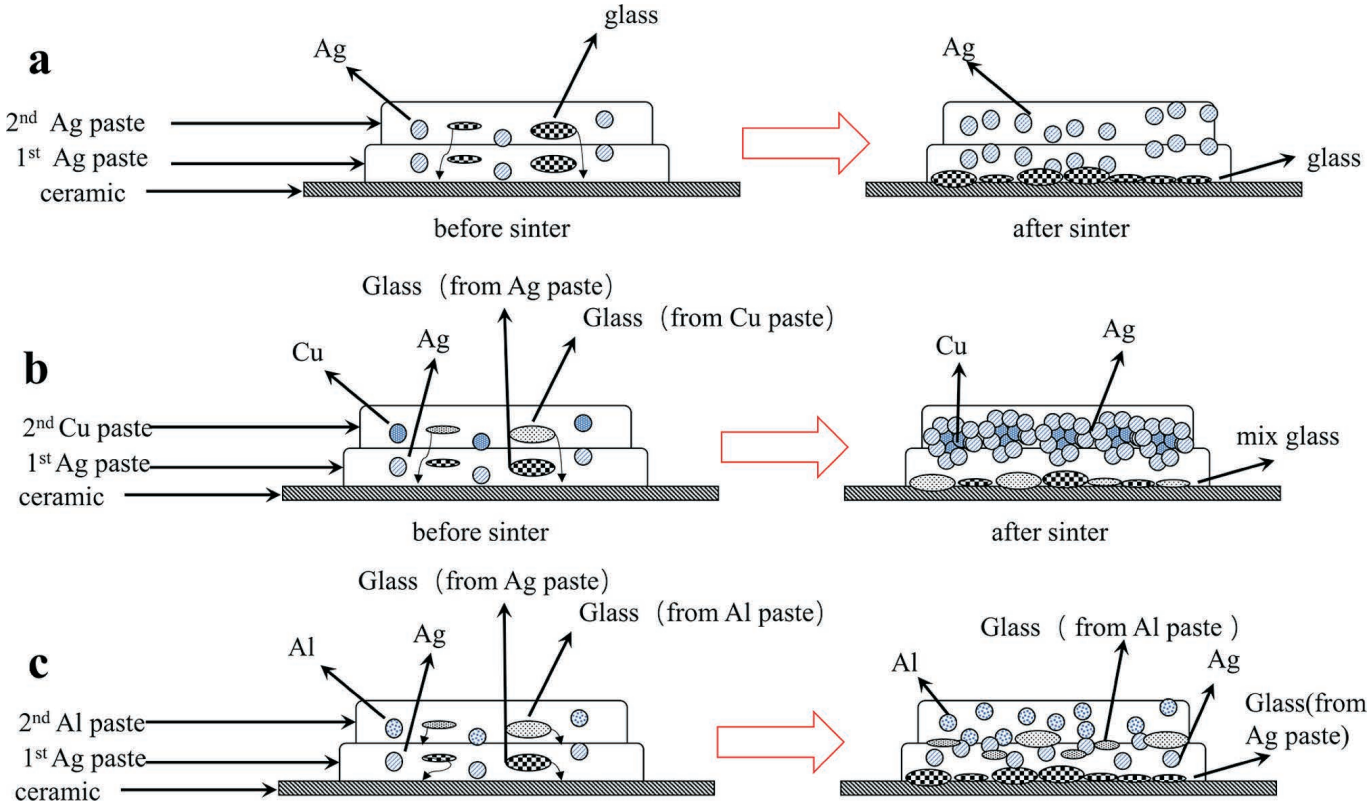

Fig. 7: The diffusion mechanism between first and second layer.

There is no obvious difference in the resistance of the three groups, which is about 1.4 Ω, only Stack 2 exhibits slightly higher resistance at 1.8 Ω. It can be seen from Fig. 3b that there is a slight oxidation problem on the surface of Cu after sintering. This is due to the effect of oxygen in the atmosphere although high-purity nitrogen was used during the experiment. However, in consideration of their cross-sectional morphology, it can be inferred that the conduction mechanism of the three systems is absolutely different. In Fig. 4 a1, although there is silicon and a few voids between the two Ag layers, the conductivity of the finished Ag layer is consistent with that of the single Ag layer, indicating that silicon and voids have little effect on the conductivity. However, physical contact between the Ag layer and the Al layer occurred, and no obvious diffusion layer was observed. Even though the Al layer itself is not dense enough, the contact between particles is sufficient. Meanwhile, the EDS analysis in Fig. 5c shows that there is Al in the Ag layer and Ag also exists in the Al layer, which may play a positive role in conduction ability. However, in the system of Cu-Ag layers (Stack 2), the conduction mechanism is quite different. The alloy formed in Stack 2 allows the conduction of the interface between Cu and Ag layers.

(4) The interface diffusion mechanism of the multi-layers

As shown in Fig. 7, after the two layers of silver are sintered, the glass phase transfers to the interface between the metal layer and the ceramic, leaving relatively complete metal silver on the upper part. However, after the sintering of the Ag-Cu interface, the silver and copper fuses together to form an alloy in the upper part, and the glass phase cannot be seen, but the metal interface of some samples is still attached to the ceramic, so it is assumed that the glass phase also diffuses to the interface between the metal layer and the ceramic substrate. There is obvious separation in the interface between silver and aluminum, only a layer of aluminum metal is formed on the basis of the thick-film silver layer, which is similar to a simple physical embedding combination, and the glass phase does not diffuse to the interface between the ceramic and metal.

IV. Conclusions

In this paper, Ag-Ag, Ag-Cu and Ag-Al multi-layer circuits have been constructed on the surface of an alumina ceramic substrate, respectively. With the help of SEM and EDS, we have revealed the interface morphology and interface diffusion mechanism of these three multi-layers. The interface of Ag-Al showed physical and mechanical occlusion, and the glass is between the two metal layers. However, in the interface of Ag-Ag and Ag-Cu, the glass phase of the two kinds of slurry diffuses between the metal layer and the ceramic substrate, the upper part formed a complete metal layer and an alloy layer, respectively. Different interface combination leads to different adhesion, and Ag-Ag showed good mechanical properties. However, the three groups of interfaces have effective electrical connection. So, the multi-layer structure is suitable for complex packaging (e.g. applied to LED) that requires stacked circuits.

References

1 Beyne, E., Mertens, R.: Trends in packaging and high density interconnection. In: ICM'99. Proceedings, Eleventh International Conference on Microelectronics. Kuwait, 1999.

2 Islam, N., Pandey, V., Kim, K.: Fine pitch Cu pillar with bond on lead (BOL) assembly challenges for low cost and high performance flip chip package. In: 2017 IEEE 67th Electronic Components and Technology Conference (ECTC). Orlando, FL, USA, 2017.

3 Yee, C.F., Jambek, A.B., Al-Hadi, A.A.: Advantages and challenges of 10-gbps transmission on high-density interconnect boards, *J. Electron. Mater.*, **45**, 3134 – 3141, (2016).

4 Calata, J.N., Bai, J.G., Liu, X., Wen, S., Lu, G.Q.: Three-dimensional packaging for power semiconductor devices and modules, *IEEE T. Adv. Packaging*, **28**, 404 – 412, (2005).

5 Reboun, J., Hlina, J., Soukup, R., Johan, J.: Printed thick copper films for power applications. In: 2018 7th Electronic System-Integration Technology Conference (ESTC). Dresden, Germany, 2018.

6 Kim, D.U., Kim, K.S., Jung, S.B.: Effects of oxidation on reliability of screen-printed silver circuits for radio frequency applications, *Microelectron. Reliab.*, **63**, 120 – 124, (2016).

7 Sanchez-Romaguera, V., Ziai, M.A., Oyeka, D., Barbosa, S., Wheeler, J.S., Batchelor, J.C., Parker, E.A., Yeates, S.G.: Towards inkjet-printed low cost passive UHF RFID skin mounted tattoo paper tags based on silver nanoparticle inks, *J. Mater. Chem. C*, **1**, 6395 – 6402, (2013).

8 Nowak, D., Miś, E., Dziedzic, A., Kita, J.: Fabrication and electrical properties of laser-shaped thick-film and LTCC microresistors, *Microelectron. Reliab.*, **49**, 600 – 606, (2009).

9 Zhang, R., Johnson, R.W., Vert, A., Zhang, T., Shaddock, D.: Assembly materials and processes for high-temperature geothermal electronic modules, *IEEE T. Comp. Pack. Man.*, **2**, 1739 – 1749, (2012).

10 Ortolino, D., Engelbrecht, A., Lauterbach, H., Bräu, M., Kita, J., Moos, R.: Effect of repeated firing on the resistance of screen-printed thick-film conductors, *J. Ceram. Sci. Tech.*, **5**, 317 – 326, (2014).

11 Vrana, M., Van Calster, A., Vanden Berghe, R.V., Allaert, K.: Interconnection technology for advanced high density thick films, *Microelectron. Int.*, **13**, 5 – 8, (1996).

12 Chan, H.Y., Fukuda, C., Yildirim, D., Li, G., Bachman, M.: Low cost, high density interposers in aluminum oxide films. In: 2016 IEEE 66th Electronic Components and Technology Conference (ECTC). Las Vegas, NV, USA, 2016.

13 Reboun, J., Hlina, J., Totzauer, P., Hamacek, A.: Effect of copper-and silver-based films on alumina substrate electrical properties, *Ceram. Int.*, **44**, 3497 – 3500, (2018).

14 Marcinkowski, M., Schmidt, R., Eberstein, M., Partsch, U.: Sinter kinetics and interface reactions of silver thick films on aluminium nitride. In: 2017 IMAPS Nordic Conference on Microelectronics Packaging (NordPac). Gothenburg, Sweden, 2017.

15 Ma, M., Liu, Z., Zhang, F., Liu, F., Li, Y.: Suppression of silver diffusion in borosilicate glass-based low-temperature cofired ceramics by copper oxide addition, *J. Am. Ceram. Soc.*, **99**, [7], 2402 – 2407, (2016).

16 Wang, Y., Alford, T.: Formation of aluminum oxynitride diffusion barriers for ag metallization, *Appl. Phys. Lett.*, **74**, [1], 52 – 54, (1999).

17 Yoo, H., Shin, H., Lee, M.: Direct patterning of double-layered metal thin films by a pulsed Nd: YAG laser beam, *Thin Solid Films*, **518**, [10], 2775 – 2778, (2010).

18 Wang, D., Mei, Y.H., Xie, H., Zhang, K., Siow, K.S., Li, X., Lu, G.Q.: Roles of palladium particles in enhancing the electrochemical migration resistance of sintered nano-silver paste as a bonding material, *Mater. Lett.*, **206**, 1 – 4, (2017).

19 Yang, C., Wu, J., Lee, C., Kao, C.: Analyses and design for electrochemical migration suppression by alloying indium into silver, *J. Mater. Sci. Mater. Electron.*, **29**, 13878 – 13888, (2018).

20 Kumm, J., Chacko, R.V., Samadi, H., Hartmann, P., Eberlein, D., Jäger, U., Wolf, A.: Long-term and annealing stable, solderable PVD metallization with optimized al diffusion barrier, *Energy Procedia*, **77**, [374.10], 1016, (2015).

21 Kumm, J., Samadi, H., Chacko, R., Hartmann, P., Wolf, A.: Analysis of al diffusion processes in TiN barrier layers for the application in silicon solar cell metallization, *J. Appl. Phys.*, **120**, [2], 025304, (2016).